Electronic Supplemental Information:

1. Experimental Section

1.1 Preparation of $ZnFe_2O_4$

Firstly, the F-SnO_2 conductive glass (FTO) was ultrasonically rinsed by CH_3COCH_3, $(CH_3)_2CHOH$, CH_3CH_2OH and deionized water, respectively. The rinsed FTO with the conductive side facing down was placed in a Teflon lined stainless steel autoclave (TLSSA). 0.15 M $FeCl_3 \cdot 6H_2O$, 0.10 M $Zn(NO_3)_2 \cdot 6H_2O$ and 0.15 M $NaNO_3$ were dissolved in 20 mL deionized water and stirred for 15 min to gain the yellow precursor solution, which was poured into the TLSSA for 6 h at 100 °C. Then, the substrate with samples was rinsed by deionized water and dried. Next, the FTO was annealed at 550 °C for 2 h. After that, the FTO was soaked in 1 M NaOH solution for 12 h to eliminate the undesirable outer-field ZnO. Finally, the pure $ZnFe_2O_4$ was fabricated successfully.

1.2 Preparation of pristine Ni-$ZnFe_2O_4$

The majority of the preparation parameters of the pristine Ni-$ZnFe_2O_4$ was resembled that of the $ZnFe_2O_4$. The discrepancy was that 0.04 M $Ni(NO_3)_2 \cdot 6H_2O$ was added into the precursor solution. Other processes were retained immutable.

1.3 Preparation of $ZnFe_2O_4$/Ni-$ZnFe_2O_4$ p-n homojunction

The FTO with $ZnFe_2O_4$ was placed in the TLSSA. 0.15 M $FeCl_3 \cdot 6H_2O$, 0.10 M $Zn(NO_3)_2 \cdot 6H_2O$, 0.15 M $NaNO_3$ and 0.04 M $Ni(NO_3)_2 \cdot 6H_2O$ were dissolved in 20 mL deionized water and agitated for 15 min to acquire the precursor solution, which was decanted into the TLSSA at 100 °C for 2 h. After that, the FTO was cleaned by deionized water and dried. And then, the FTO was heat-treated at 550 °C for 2 h. After the heat-treatment, the FTO was stepped in 1 M NaOH solution for 12 h aim at purification. Finally, the $ZnFe_2O_4$/Ni-$ZnFe_2O_4$ p-n homojunction was prepared.

1.4 Characterizations

The surface morphology of samples was observed by JEOL JSM-7800F scanning electron microscope (SEM). The microstructure of samples was carried out by JEOL JEM-2100 transmission electron microscopy (TEM). The crystallographic phase identification of samples was studied by X-ray diffractometer (XRD, Rigaku-D/max-2500; Cu Kα radiation, λ=0.154059 nm, 40 kV). The element composition of samples was measured by energy dispersive X-ray spectroscopy (EDS, AZtec from Oxford). The chemical state of samples was determined by X-ray photoelectron spectroscopy (XPS, Thermo ESCALAB 250Xi). The optical absorption property of

samples was characterized by DU-8B UV-vis double-beam spectrophotometer. The PEC performance of as-prepared samples was measured by electrochemical workstation (CHI760E), while 0.5 M Na_2SO_4 aqueous solution without sacrificial agent (pH=7) was used as electrolyte, a standard three-electrode configuration includes working electrode (as-prepared samples), counter electrode (platinum foil) and reference electrode (Ag/AgCl electrode) illuminated with a Xenon lamp (100 mW/cm^2). The electrochemical impedance spectra (EIS) of samples was performed on a three-electrode configuration, tested under illumination at a potential of 0 V vs RHE and a frequency range of 10-100 kHz. The optical band gap of samples was calculated as follows:

$$(\alpha h\upsilon)^n = A(h\upsilon - E_g) \quad (1)$$

Where α was the absorption coefficient, h was the Planck's constant, υ was the photon frequency, the n was 2 since $ZnFe_2O_4$ was to a direct band gap semiconductor, A was a constant and E_g was the optical band gap.

The Mott-Schottky plot of samples was characterized in 0.5 M Na_2SO_4 electrolyte to assess the flat band potential of samples, and p-n characteristic, the calculation process was according to the following equations:

$$n\text{-type semiconductor}: 1/C^2 = (2/e_0\varepsilon\varepsilon_0 N_d)[(V_a - V_{fd}) - kT/e_0] \quad (2)$$

$$p\text{-type semiconductor}: 1/C^2 = (2/e_0\varepsilon\varepsilon_0 N_A)[(-V_a + V_{fd}) - kT/e_0] \quad (3)$$

Where C was the specific capacitance, e_0 was fundamental electric charge, ε was the dielectric constant, ε_0 was the permittivity of vacuum, N_d was the donor density (n-type semiconductor), N_A was the acceptor density (p-type semiconductor), V_a was the applied potential, V_{fd} was the flat band potential, k was the Boltzmann constant and T was the temperature. In order to clarify the charge separate dynamics in bulk and surface, we determine the charge separation efficiency in the bulk (η_{bulk}) and on the surface ($\eta_{surface}$) through adding 0.1M Na_2SO_3 hole scavenger in 0.5M Na_2SO_4 electrolyte solution. η_{bulk} is calculated by the equation as following [1,2]:

$$J_{H2O} = J_{abs} \times \eta_{bulk} \times \eta_{surface} \quad (4)$$

Where J_{H2O} was the photocurrent density measured without Na_2SO_3 (just Na_2SO_4 aqueous solution, 0.5M) at 1.23 V vs. RHE, J_{abs} was the photocurrent density generated when all photons absorbed by samples were converted into electrons and holes, the J_{abs} values of $ZnFe_2O_4$, Ni-$ZnFe_2O_4$ and $ZnFe_2O_4$/Ni-$ZnFe_2O_4$ were calculated as 4.27 mA/cm^2, 4.37 mA/cm^2 and 4.31 mA/cm^2 according to the references of [3] and [4], respectively. With adding 0.1M Na_2SO_3 as the electrolyte,

the oxidation kinetics of the system is very rapid so that fundamentally suppresses the surface recombination of charge carriers without influencing the bulk charge separation, thus, $\eta_{surface}$ could be regarded as 100%. Therefore, the photocurrent density in the presence of Na_2SO_3 is calculated as following:

$$J_{H2O} = J_{abs} \times \eta_{bulk} \quad (5)$$

As a consequence, the charge separation efficiency of samples was obtained according to the following equations:

$$\eta_{bulk} = J_{Na2SO3}/J_{abs} \times 100\% \quad (6)$$

$$\eta_{surface} = J_{H2O}/J_{Na2SO3} \times 100\% \quad (7)$$

J_{Na2SO3} was the photocurrent density measured with Na_2SO_3 photo-oxidation (Na_2SO_4/Na_2SO_3 aqueous solution, 0.5M/0.1M). The measured data for calculating the bulk and surface charge separation efficiency was shown in Fig.S8. The Ag/AgCl potential was transformed to the reversible hydrogen electrode (RHE) potential according to the following formula:

$$E_{RHE} = E_{Ag/AgCl} + 0.059pH + 0.1976 \quad (8)$$

References:

[1] K. H. Ye, Z. Wang, J. Gu, S. Xiao, Y. Yuan, Y. Zhu, Y. Zhang, W. Mai, S. Yang, *Energy Environ. Sci.*, 2017, 10, 772-779.

[2] H. Dotan, K. Sivula, M. Grätzel, A. Rothschild, S. C. Warren, *Energy Environ. Sci.*, 2011, 4, 958-964.

[3] J. H. Kim, J. H. Kim, J. W. Jang, J. Y. Kim, S. H. Choi, G. Magesh, J. Lee, J. S. Lee, *Adv. Energy Mater.*, 2015, 5, 1401933.

[4] H. W. Jeong, T. H. Jeon, J. S. Jang, W. Choi, H. Park, *J. Phys. Chem. C*, 2013, 117, 9104-9112.

List of Figures:

Fig.S1 Synthetic route schematic diagram of $ZnFe_2O_4$/Ni-$ZnFe_2O_4$ p-n homojunction

Fig.S2 Cross-view SEM images of $ZnFe_2O_4$ (a), Ni-$ZnFe_2O_4$ (b), $ZnFe_2O_4$/Ni-$ZnFe_2O_4$

Fig.S3 Element distribution mapping of $ZnFe_2O_4$/Ni-$ZnFe_2O_4$ p-n homojunction

Fig.S4 XRD patterns of samples

Fig.S5 TEM image (a) and HRTEM image (b) of $ZnFe_2O_4$/Ni-$ZnFe_2O_4$ core-shell p-n homojunction

Fig.S6 XPS valence band spectra (a) and Valence/Conduction Band sketch map (b) of samples

Fig.S7 Mott-Schottky plots of $ZnFe_2O_4$ (a) and Ni-$ZnFe_2O_4$ (b)

Fig.S8 The J-V curves of $ZnFe_2O_4$, Ni-$ZnFe_2O_4$ and $ZnFe_2O_4$/Ni-$ZnFe_2O_4$ with/without Na_2SO_3

Fig.S9 Equivalent circuit model (a) and related parameters of electrochemical impedance spectra (b) of samples

Fig.S10 Charge transfer mechanism iagram of $ZnFe_2O_4$/Ni-$ZnFe_2O_4$ core-shell p-n homojunction

Fig.S11 Brief diagram of p-n junction: (a) single semiconductor, (b) forming p-n junction, (c) charge transfer of p-n junction under illumination

Tab.S1 Summary of XPS data about Zn 2p, Fe 2p, O 1s, Ni 2p and C 1s of $ZnFe_2O_4$/Ni-$ZnFe_2O_4$

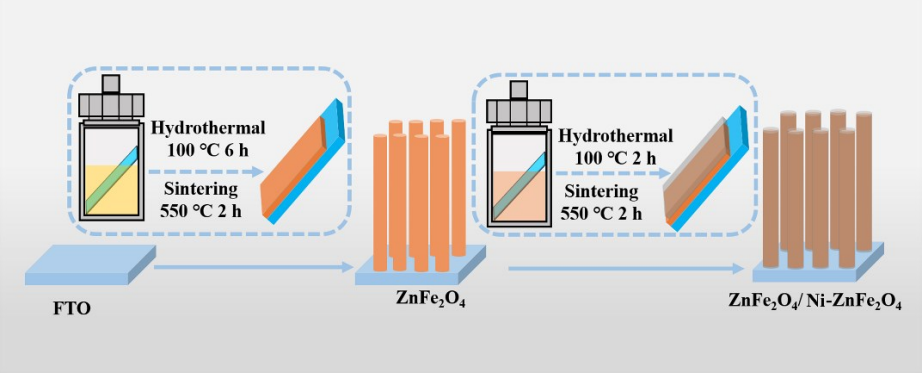

Fig.S1 Synthetic route schematic diagram of $ZnFe_2O_4$/Ni-$ZnFe_2O_4$ p-n homojunction

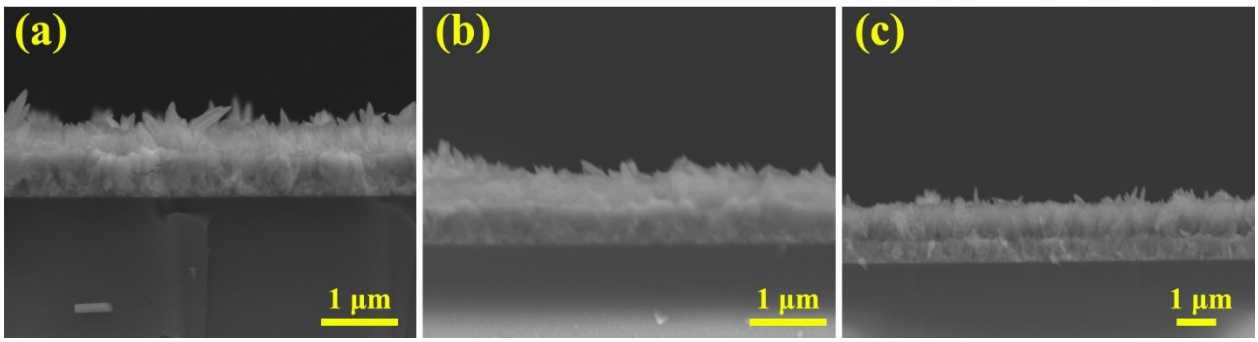

Fig.S2 Cross-view SEM images of $ZnFe_2O_4$ (a), Ni-$ZnFe_2O_4$ (b), $ZnFe_2O_4$/Ni-$ZnFe_2O_4$

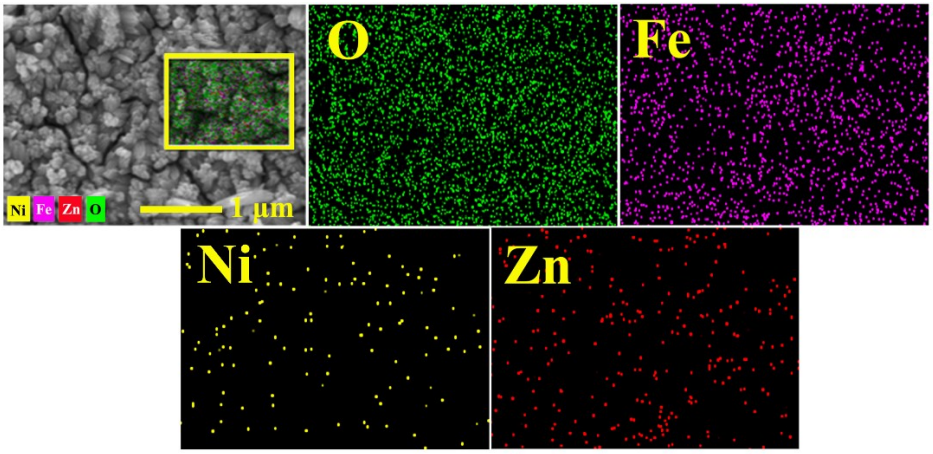

Fig.S3 Element distribution mapping of $ZnFe_2O_4$/Ni-$ZnFe_2O_4$ p-n homojunction

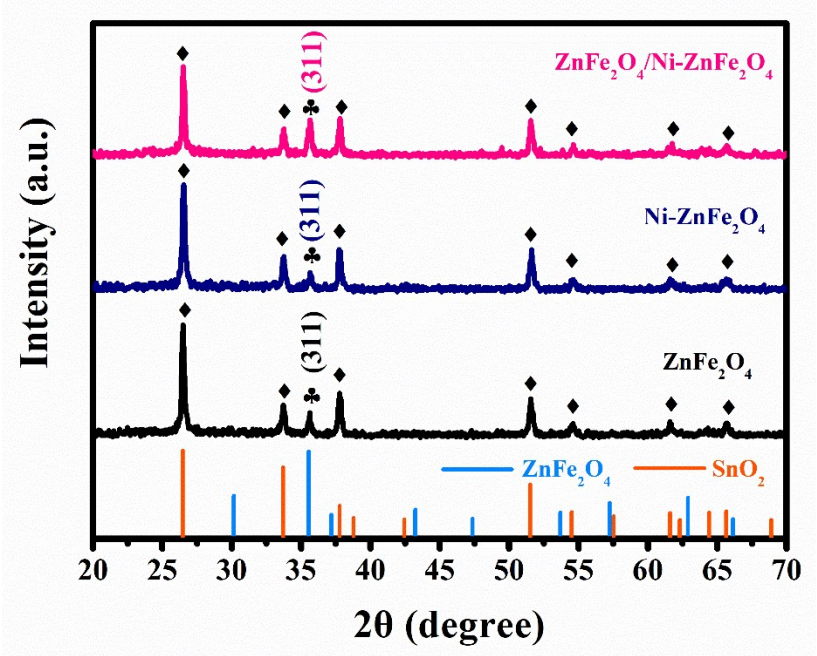

Fig.S4 XRD patterns of samples

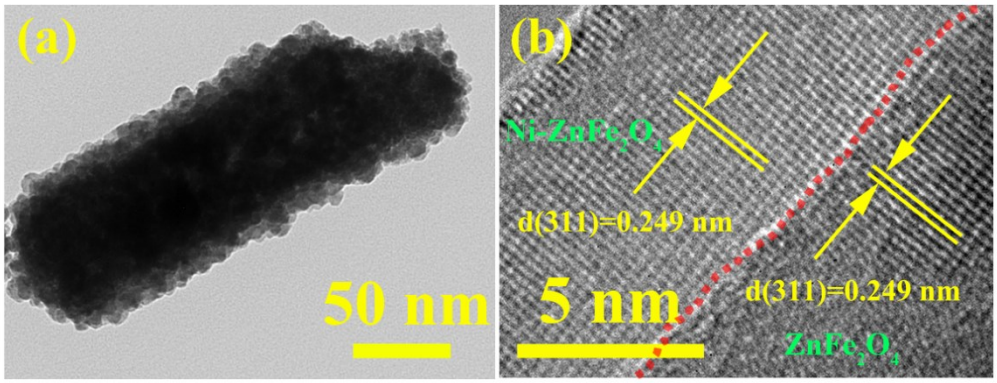

Fig.S5 TEM image (a) and HRTEM image (b) of $ZnFe_2O_4$/Ni-$ZnFe_2O_4$ core-shell p-n homojunction

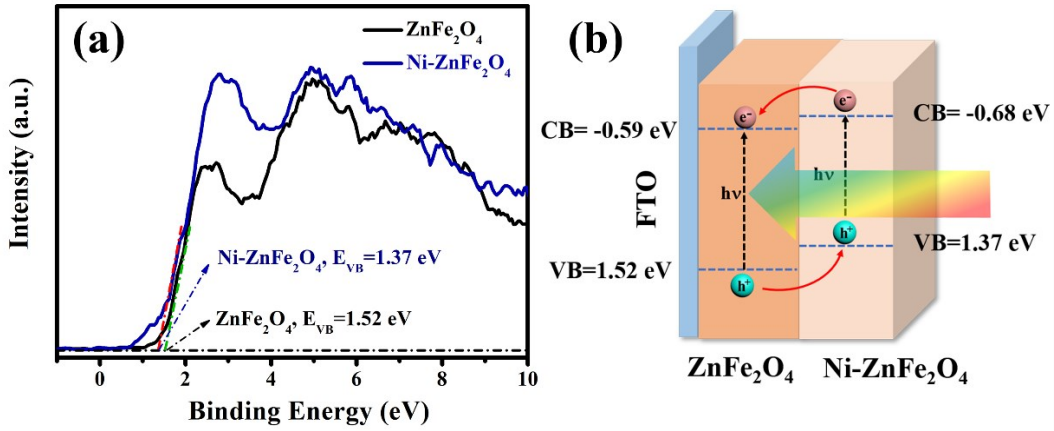

Fig.S6 XPS valence band spectra (a) and Valence/Conduction Band sketch map (b) of samples

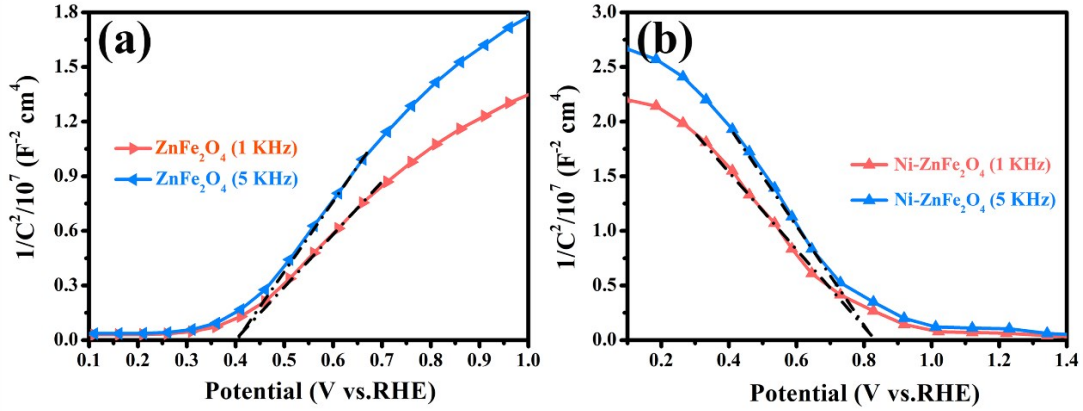

Fig.S7 Mott-Schottky plots of $ZnFe_2O_4$ (a) and Ni-$ZnFe_2O_4$ (b)

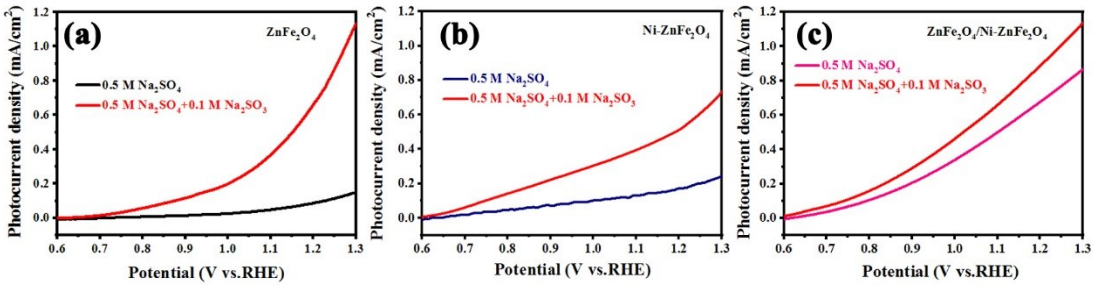

Fig. S8 The J-V curves of $ZnFe_2O_4$, Ni-$ZnFe_2O_4$ and $ZnFe_2O_4$/Ni-$ZnFe_2O_4$ with/without Na_2SO_3

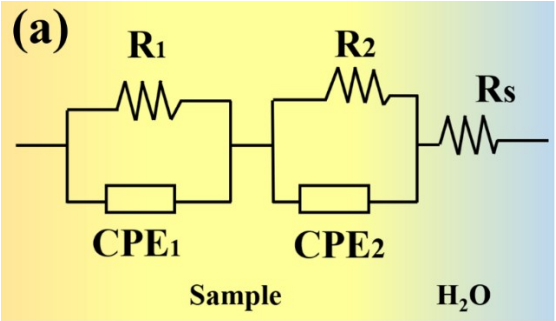

(b)

Sample	R_1 (Ω)	R_2 (Ω)	R_s (Ω)
$ZnFe_2O_4$	6898.63	1371.52	27.94
Ni-$ZnFe_2O_4$	6425.18	1149.87	26.37
$ZnFe_2O_4$/Ni-$ZnFe_2O_4$	6058.63	942.36	25.29

Fig.S9 Equivalent circuit model (a) and related parameters of electrochemical impedance spectra (b) of samples

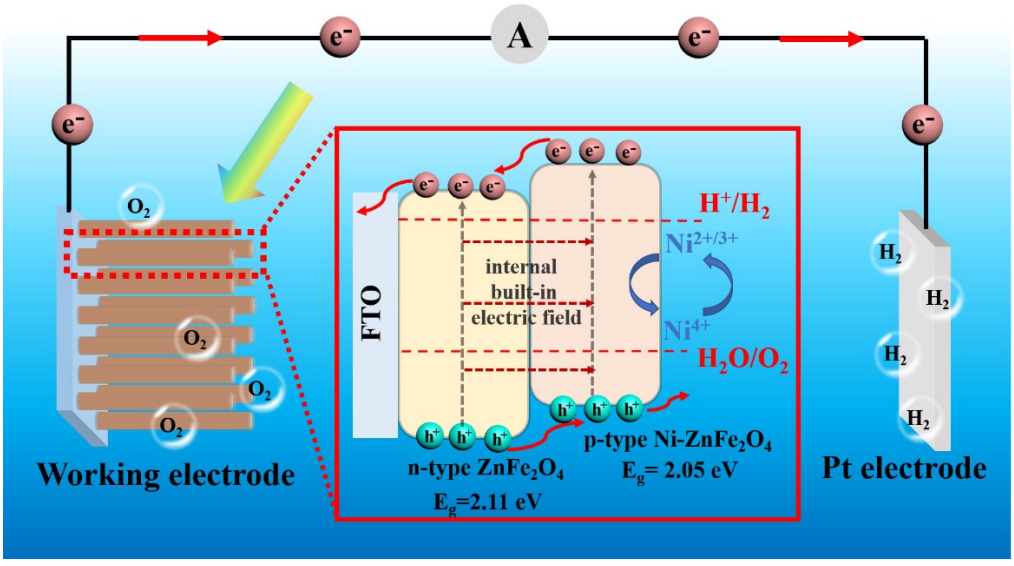

Fig.S10 Charge transfer mechanism diagram of $ZnFe_2O_4$/Ni-$ZnFe_2O_4$ core-shell p-n homojunction

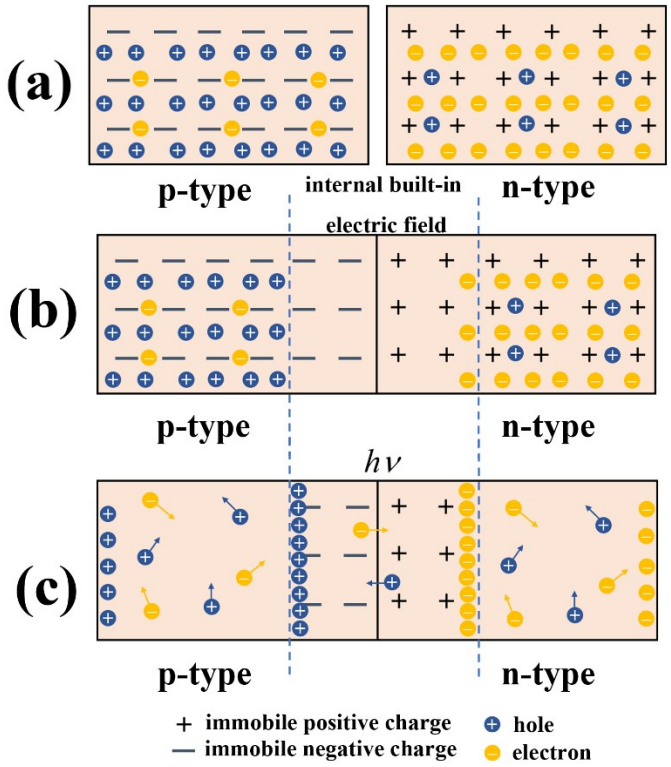

Fig.S11 Brief diagram of p-n junction: (a) single semiconductor, (b) forming p-n junction, (c) charge transfer of p-n junction under illumination

Tab.S1 Summary of XPS data about Zn 2p, Fe 2p, O 1s, Ni 2p and C 1s of $ZnFe_2O_4$/Ni-$ZnFe_2O_4$

Name	Atomic %	Start BE	End BE	Peak BE	Peak Type
Zn 2p	11.63	1059.15	1008.62	1022.7	Standard
Fe 2p	23.26	747.01	697.29	710.8	Standard
O 1s	46.52	540.23	524.85	529.8	Standard
Ni 2p	1.97	891.81	840.75	855.6	Standard
C 1s	16.62	296.37	281.61	284.7	Standard